Structure of turbulence in temporal planar jets

Cite as: Phys. Fluids **34**, 045109 (2022); https://doi.org/10.1063/5.0085091
Submitted: 12 January 2022 • Accepted: 20 March 2022 • Published Online: 06 April 2022

A. Cimarelli, A. Fregni, J.-P. Mollicone, et al.

Physics of Fluids ARTICLE scitation.org/journal/phf

Structure of turbulence in temporal planar jets

Cite as: Phys. Fluids **34**, 045109 (2022); doi: 10.1063/5.0085091
Submitted: 12 January 2022 · Accepted: 20 March 2022 ·
Published Online: 6 April 2022

A. Cimarelli,[1,a)] A. Fregni,[2] J.-P. Mollicone,[3] M. van Reeuwijk,[4] and E. De Angelis[2]

AFFILIATIONS

[1]DIEF, University of Modena and Reggio Emilia, 41125 Modena, Italy
[2]School of Engineering, Cardiff University, Cardiff CF24 3AA, United Kingdom
[3]Faculty of Engineering, University of Malta, Msida MSD 2080, Malta
[4]Department of Civil and Environmental Engineering, Imperial College London, SW7 2AZ London, United Kingdom

[a)]Author to whom correspondence should be addressed: andrea.cimarelli@unimore.it

ABSTRACT

A detailed analysis of the structure of turbulence in a temporal planar turbulent jet is reported. Instantaneous snapshots of the flow and three-dimensional spatial correlation functions are considered. It is found that the flow is characterized by large-scale spanwise vortices whose motion is felt in the entire flow field. Superimposed to this large-scale motion, a hierarchy of turbulent structures is present. The most coherent ones take the form of quasi-streamwise vortices and high and low streamwise velocity streaks. The topology of these interacting structures is analyzed by quantitatively addressing their shape and size in the different flow regions. Such information is recognized to be relevant for a structural description of the otherwise disorganized motion in turbulent free-shear flows and can be used for the assessment of models based on coherent structure assumptions. Finally, the resulting scenario provides a phenomenological description of the elementary processes at the basis of turbulence in free-shear flows.

I. INTRODUCTION

Research on turbulence generally aims at providing a description of the phenomenon that is simpler than that given by the Navier–Stokes equations. To this purpose, almost every approach to turbulence is essentially based on a decomposition of the turbulent field. Historically, famous examples are the Reynolds decomposition in a mean and fluctuating flow and the spectral decomposition in a hierarchy of scales of motion. More recently, research efforts often rely on the decomposition of turbulence in random processes and coherent structures.[1] The interest is in describing turbulence in terms of a small number of relevant elementary processes.

In the present work, we aim at identifying and characterizing such relevant structures of turbulence in free-shear flows by using direct numerical simulation (DNS) data of a temporal planar turbulent jet. In the context of free-shear flows, the assessment of the statistically relevant structure of turbulence[2–7] is of importance for a number of scientific and applicative issues. An example is the study of turbulent entrainment.[8,9] It is well-known that entrainment is not only diffusion of vorticity at the turbulent interface. Indeed, it is widely accepted that entrainment is also the result of engulfment processes of irrotational fluid and, hence, of large-scale coherent motions.[10–12] In particular, the anisotropy induced by large-scale structures was found in Cimarelli and Boga[13] to represent a fundamental phenomenon for the effective sustainment of the entrainment and mixing processes. Another example is the modeling of the interaction mechanisms between large and small scales in a context of Large Eddy Simulation.[14–16] As shown in da Silva and Mètais,[17] the most intense energy exchanges between large and small scales are related to the presence of coherent structures in the flow, such as spanwise and longitudinal vortices. From an application point of view, the identification of the coherent structure of turbulence is highly relevant for flow control. A structural representation of turbulence is indeed known to be effective in identifying the action mechanisms to manipulate specific turbulence properties.[18,19]

The study of the structure of turbulence in free-shear flows dates back some time ago. Jiménez[20] showed that superimposed on the primary spanwise vortex structure of plane mixing layers, a second instability develops in the form of an undulation of the primary vortex core. This picture was later refined by Bernal and Roshko,[21] where this deformation was shown to evolve in longitudinal vortex structures, see also Liepmann and Gharib,[4] Nogueira *et al.*[22] The structure of turbulence in free-shear layers has been also analyzed in flows with separation. In this context, it is shown that the flow first develops spanwise vortices as a result of the two-dimensional shear instability. Perturbations of the flow field lead to a lift up and stretching of the primary spanwise vortices, thus forming hairpin-like structures[23] that by

flowing downstream undergo stretching giving rise to streamwise vortices.[24] As shown by Lasheras and Choi,[25] streamwise vortices are then found to induce entrainment and streamwise velocity streaks. More recently, this picture has been quantitatively assessed in Cimarelli *et al.*[26] by means of a statistical analysis of three-dimensional spatial velocity correlation.

The present work is devoted to the statistical characterization of the structure of turbulence in the plane shear layers developed in a temporal jet. We start by reporting the numerical settings adopted for the direct numerical simulation in Sec. II A and by briefly describing the main flow features in Sec. II B. Important considerations on the domain size are reported in Sec. II C. The structure of turbulence is analyzed first in Sec. III by addressing the instantaneous flow topology. Then, in Sec. V, a characterization of the statistically relevant flow structures is reported by means of a detailed analysis of the three-dimensional spatial velocity correlation functions that in turn are defined in Sec. IV. The work is closed by final remarks in Sec. VI.

II. TURBULENT TEMPORAL JET

A. Direct numerical simulation

In the present work, we consider direct numerical simulation (DNS) data of a temporal plane jet performed by solving the Navier–Stokes equations coupled with the evolution equation of a passive scalar,

$$\begin{aligned} \frac{\partial u_i}{\partial x_i} &= 0, \\ \frac{\partial u_i}{\partial t} + \frac{\partial u_i u_j}{\partial x_j} &= -\frac{\partial p}{\partial x_i} + \frac{1}{Re}\frac{\partial^2 u_i}{\partial x_j \partial x_j}, \\ \frac{\partial \theta}{\partial t} + \frac{\partial \theta u_j}{\partial x_j} &= \frac{1}{ReSc}\frac{\partial^2 \theta}{\partial x_j \partial x_j}. \end{aligned} \tag{1}$$

Equation (1) is written in a dimensionless form by using the initial jet half-width H, the initial jet centerline velocity U_0 and the initial centerline scalar concentration Θ_0. Here, $Re = U_0 H/\nu$ is the Reynolds number, where ν is the kinematic viscosity while $Sc = \nu/\alpha$ is the Schmidt number where α is the diffusivity of the scalar. The indices $i = 1, 2, 3$ correspond to the streamwise, spanwise, and cross-flow velocities (u, v, w) and directions (x, y, z), respectively. The numerical method used to solve the problem is based on a finite volume discretization of the governing equations, see Craske and van Reeuwijk[27] for details. The symmetry-preserving method of Verstappen and Veldman[28] is employed, thus allowing for mass, momentum, and energy conservation and for a fourth-order accuracy. To advance the solution in time a third-order variable-time step, Adams–Bashforth scheme is finally used.

Periodic boundary conditions are imposed in the streamwise and spanwise directions, free-slip on the cross-flow boundaries. The initial condition is a fluid layer that is quiescent and characterized by a null concentration of the scalar except for a thin region $-H < z < H$ where the streamwise velocity and the scalar are non-zero and homogeneously distributed in the streamwise and spanwise directions,

$$\begin{aligned} u(x, y, z, 0) &= \frac{U_0}{2}\left[1 + \tanh\left(\frac{H - |z|}{2\sigma_0}\right)\right], \\ \theta(x, y, z, 0) &= \frac{\Theta_0}{2}\left[1 + \tanh\left(\frac{H - |z|}{2\sigma_0}\right)\right], \end{aligned} \tag{2}$$

where $\sigma_0 = 2H/35$ is the initial momentum thickness. In order to facilitate a rapid transition to turbulence, a perturbation is superimposed at the initial conditions (2) consisting in a uniform random noise with an intensity that is 4% the maximum initial velocity.

The flow problem considered here is for $Re = 1000$ and $Sc = 1$. The computational domain is a cuboid of size $96H \times 96H \times 48H$ and has been discretized by using $2304 \times 2304 \times 960$ uniformly spaced grid points. By using the smallest value of the Kolmogorov scale η_{min} obtained at the centerline of the jet for $t = 40$, the corresponding resolution is $\Delta x = \Delta y \approx 1.66\eta_{\min}$ and $\Delta z \approx 2\eta_{\min}$. By considering that the Kolmogorov scale increases from this minimum in time as $\sqrt{t}$ and with the cross-flow position z since dissipation is maximum at the centerline, the resolution adopted is considered appropriate for a DNS. Finally, a variable time step was used for the temporal integration in order to obtain a condition $CFL < 0.3$. The total integration time for each simulation is $t = 160$.

Starting from the same initial conditions (2) except for the perturbation superimposed, three simulations have been performed in order to provide three statistically independent samples for the ensemble average. In fact, average quantities denoted as $\langle\cdot\rangle$ are computed by performing an ensemble average between the different flow realizations, a spatial average in the statistically homogeneous streamwise and spanwise directions and by taking advantage of the statistical symmetry of the flow in the cross-flow direction. Accordingly, the average of a generic quantity β is defined as

$$\begin{aligned} \langle\beta\rangle(z, t) = \frac{1}{N}\sum_{i=1}^{N}\frac{1}{2}\Bigg(&\frac{1}{L_x L_y}\int\int \beta(x, y, z, t)\, dxdy \\ &\pm \frac{1}{L_x L_y}\int\int \beta(x, y, -z, t)\, dxdy\Bigg), \end{aligned} \tag{3}$$

where the sum and difference of the two integrals are imposed by the symmetric/antisymmetric nature of the considered variable, L_x and L_y are the domain dimensions in the homogenous directions, and $N = 3$ is the number of independent flow samples used.

In what follows, the customary Reynolds decomposition of the flow in a mean and fluctuating field will be adopted, i.e., $u_i = U_i + u_i'$ and $\theta = T + \theta'$. In order to take into account the self-similar behavior of the flow, variables will be presented dimensionless by using the mean centerline velocity $U_{cl}(t) = U(0, t)$ and the jet half-width $h_\Omega(t)$, defined as the jet centerline distance where the mean enstrophy profile reaches 2% of its centerline value. The related non-dimensional flow variables will be denoted with a superscript $*$.

B. Main flow features

As shown in van Reeuwijk and Holzner[29] and da Silva and Pereira,[30] after an initial transient when the system develops turbulence, the flow approaches a self-similar regime while decaying. This dynamic equilibrium is characterized by an increase in the jet length scales as $\sim\sqrt{t}$ and by a decrease in the jet velocity scales as $\sim 1/\sqrt{t}$. As shown in Cimarelli *et al.*[31] where the same data-set is used, all the flow observables are found to follow this self-similar scaling for $t > 60$. Accordingly, flow statistics are here reported for $t = 120$, thus allowing us to characterize the flow structure in the self-similar regime. A constant Taylor Reynolds number, $Re_\lambda = \sqrt{2k_{cl}/3}\lambda_{cl}/\nu = 50$, is also achieved in the self-similar regime, where k_{cl} is the centerline turbulent

kinetic energy and $\lambda = \sqrt{10\nu k_{cl}/\varepsilon_{cl}}$ is the Taylor microscale with ε_{cl} the centerline turbulent dissipation. This intermediate value of the Reynolds number is probably not high enough to observe a complete small-scale mixing.[32–34] It is, however, sufficiently high to observe and study the large-scale coherent structures of the flow and their interactions as demonstrated in the rest of the work.

In Fig. 1(a), the mean velocity and turbulent kinetic energy profiles, $U^*(z)$ and $k^*(z)$, respectively, are shown. The inner part of the jet is characterized by high levels of velocity and turbulent kinetic energy. Moving away from the jet centerline, the mean velocity decreases while the turbulent kinetic energy increases reaching a maximum for $z^* \approx 0.3$. This region of the flow is also characterized by the highest values of mean shear and, as shown in Cimarelli *et al.*,[31] of turbulence production. By further increasing the jet centerline distance, both the mean shear and the turbulent kinetic energy decrease asymptotically reaching zero values in the external region of the jet.

The one-dimensional streamwise turbulent spectrum evaluated in the production region at $z^* = 0.35$ is shown in Fig. 1(b). As shown in the main plot, the spectrum of fluctuations exhibits a small inertial range, less than one decade, where the power law $k_x^{-5/3}$ is followed. This range takes origin from very large length scales of the order of $\lambda_x^* = 2\pi/k_x^* \approx 1.5$ and is followed by a viscosity-dominated scaling for $\lambda_x^* < 0.2$. As shown in the inset panel of Fig. 1(b), the premultiplied streamwise turbulent spectrum highlights that the length scale $\lambda_x^* \approx 1.5$ origin of the inertial range scaling is also the most energetic one. It is worth noting that this relevant length scale is larger than the jet half-width h_Ω, thus highlighting the relevance of using large computational domains in order to correctly capture the turbulence dynamics of temporal jets. This aspect is further addressed in Sec. II C.

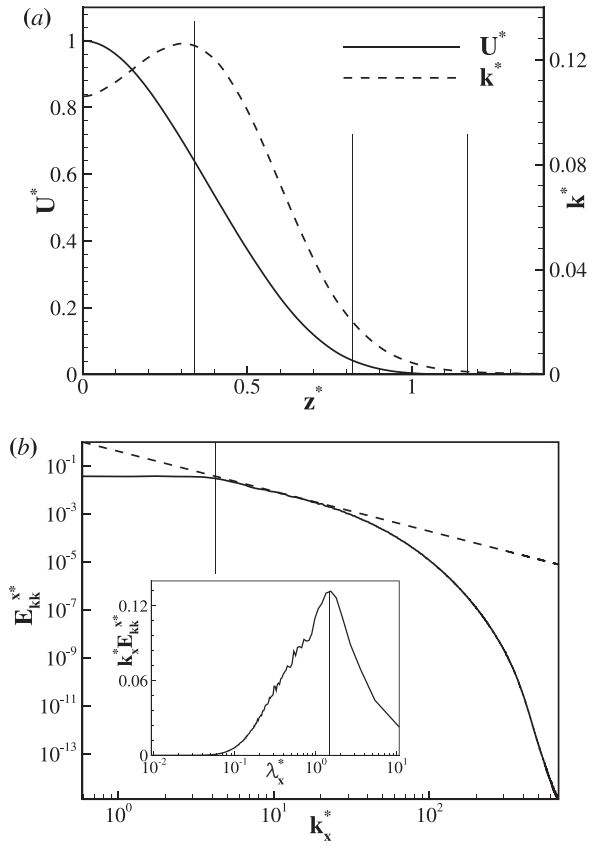

FIG. 1. (a) Mean velocity and turbulent kinetic energy profiles, $U^*(z)$ and $k^*(z)$, respectively. The vertical lines denote the locations used for the analysis of the three-dimensional spatial correlation function reported in Sec. V. (b) Streamwise turbulent spectrum E_{kk}^{x*} evaluated at $z^* = 0.35$. The dashed line reports the $k_x^{-5/3}$ law. The inset panel shows the premultiplied streamwise turbulent spectrum $k_x^* E_{kk}^{x*}$ as a function of the wavelength λ_x^* evaluated at the same position and time. The vertical lines denote the value $\lambda_x^* = 2\pi/k_x^* = 1.5$.

C. Effect of the domain size

The study of the topology of turbulence requires a detailed verification of the influence of the numerical domain extent on the flow structures. To address this issue, in the present section flow variables will be presented dimensionless by using the initial jet half-width H for lengths and the initial jet centerline velocity U_0 for velocities, i.e., the numerically solved flow variables presented in Sec. II A. Indeed, in numerical simulations, H and U_0 are prescribed with the initial conditions and, hence, can be used to define a suitable dimensionless form for the equations of motion and for the domain dimensions.

The computational domain used in the present work has dimensions $96 \times 96 \times 48$, see again Sec. II A. This domain is significantly larger than the $24 \times 24 \times 36$ domain used in van Reeuwijk and Holzner[29] and even more than the $8 \times 8 \times 12$ domain used in da Silva and Pereira.[30] To verify the need of such a very large domain, we have performed two additional simulations with the same numerical settings but different domain lengths, specifically $24 \times 24 \times 36$ and $72 \times 48 \times 36$.

In Fig. 2, the instantaneous vorticity pattern of the simulations with the larger and smaller domain is shown for $t = 120$. The simulation with the larger domain (top plots) clearly highlights that the fine scale of turbulence is superimposed to very-large motions. As better shown in Sec. III, these motions induce large-scale meandering of the turbulent jet region. On the contrary, the simulation with the smaller domain (bottom plots) does not allow to reproduce such a large-scale spatial modulation of the turbulent jet core. The spatial interaction mechanisms between consecutive large-scale vortex motions cannot be reproduced in the smaller domain. In this case, large-scale motions emerge only through large-scale unsteadiness in time, thus, suppressing the spatial instability mechanisms observed in the simulation with the larger domain. On the contrary, the small scale motion does not appear to be significantly affected by the domain size.

The suppression of large-scale mechanisms due to a limited numerical domain extent strongly impacts the structure of the flow. To analyze this issue, we consider the spatial correlation function of streamwise, spanwise, and cross-flow velocity, R_{uu}, R_{vv}, and R_{ww}, respectively, evaluated at the jet centerline for $t = 120$. See Sec. IV for the definition. As shown in Fig. 3, significant differences in terms of correlation lengths and shapes by varying the domain size are present. In particular, only the largest domain size appears to show a clear decorrelation of the velocity field. Also the intermediate domain extent is found to allow for a decorrelation of the velocity field with small differences with respect to the behavior observed in the larger domain extent. On the contrary, the smaller domain extent is found to produce a substantially different large-scale flow. In particular, the streamwise velocity fluctuations do not decorrelate in the streamwise direction and shows an artificial positive peak for spanwise scales $r_y \approx 8$.

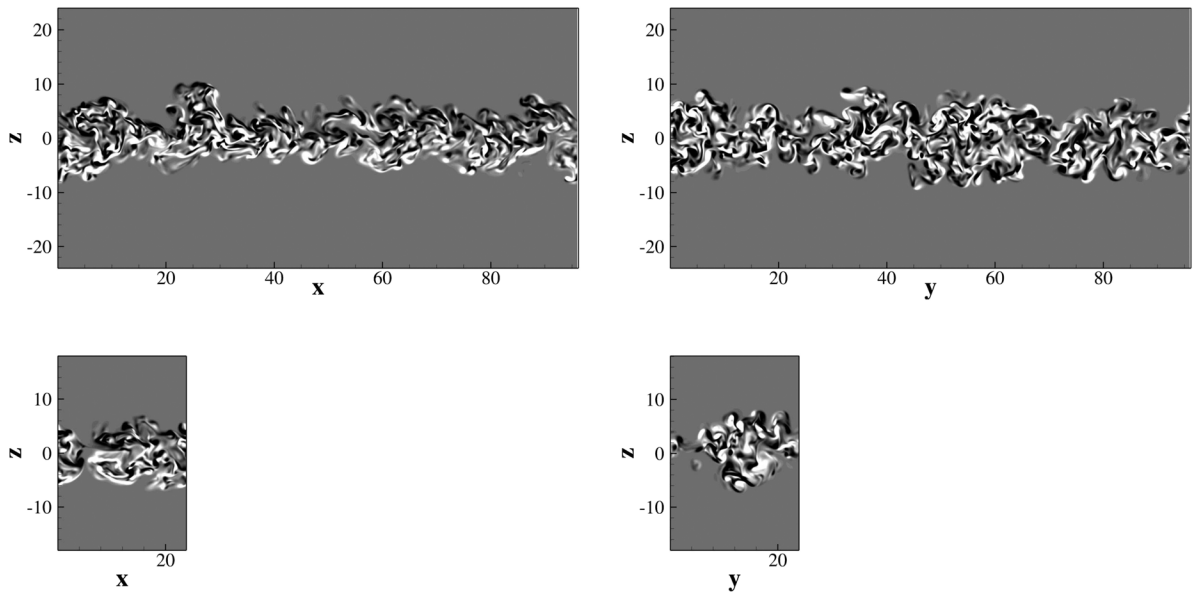

FIG. 2. Instantaneous vorticity pattern ω for the simulations with the larger (top) and smaller (bottom) domain extent evaluated at $t = 120$. The left plots show a y-plane view of the spanwise vorticity, $\omega_y \in [-0.2, 0.2]$. The right plots show a x-plane view of the streamwise vorticity, $\omega_x \in [-0.2, 0.2]$.

Also the spanwise velocity fluctuations exhibit artificial negative and positive peaks for streamwise scales $r_x \approx 3$ and $r_x \approx 8$, respectively, and do not exhibit decorrelation both in the streamwise and spanwise directions. Finally, the cross-flow fluctuations show an unnatural negative peak of correlation for spanwise scales $r_y \approx 7$.

These results clearly highlight the need of using large domain extents in order to capture the statistically relevant large-scale structures of the flow. In order to highlight the relevance of this information for the common practice, let us recall that the smaller domain extent analyzed here is the same used in van Reeuwijk and Holzner[29] that is

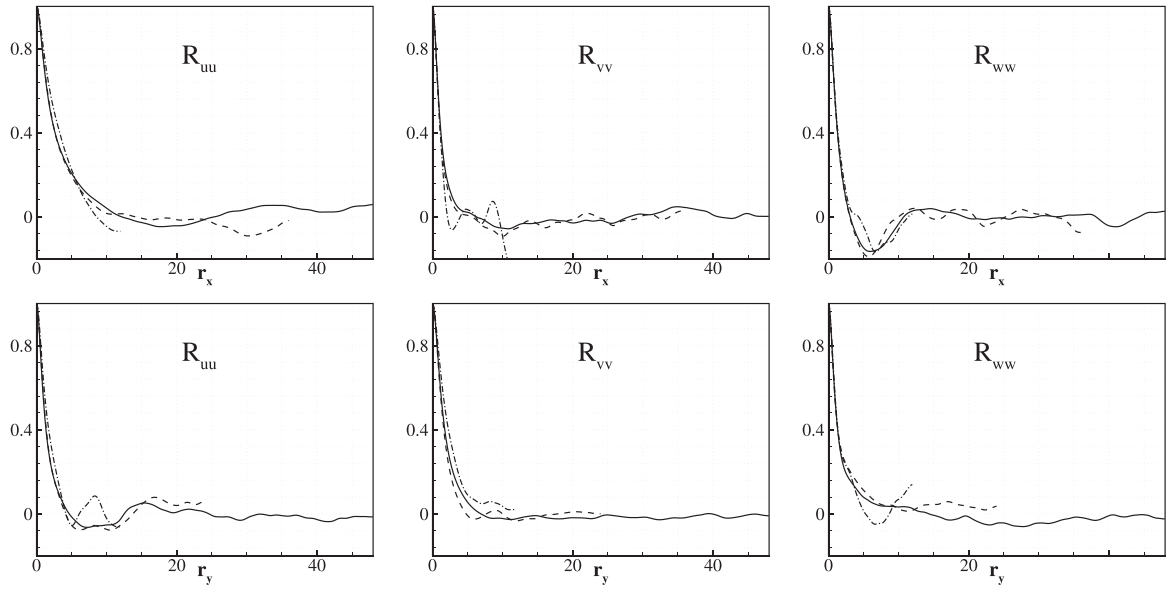

FIG. 3. Spatial correlation functions evaluated at the jet centerline for $t = 120$ for the simulations with large (solid line), intermediate (dashed line), and small (dashed-dotted line) domain. The spatial correlation is computed for the streamwise (left plots), spanwise (central plots), and cross-flow (right plots) velocity fluctuations, i.e., R_{uu}, R_{vv}, and R_{ww}, respectively. The spatial correlation is shown as a function of the streamwise separation $\boldsymbol{r} = (r_x, 0, 0)$ (top plots) and of the spanwise separation $\boldsymbol{r} = (0, r_y, 0)$ (bottom plots).

three times larger in each direction than that adopted in da Silva and Pereira.[30] Finally, let us emphasize that the use of very large domains also allows to substantially improve the statistical convergence.

III. INSTANTANEOUS FLOW PATTERN

In this section, we further analyze the instantaneous structures of the flow. Figure 4 shows iso-surfaces of the three-dimensional swirl $\boldsymbol{\omega} \cdot \boldsymbol{u}/|\boldsymbol{u}|$ of the temporal jet. A very complex pattern appears. As highlighted by the inset, these swirling motions are predominantly aligned with the axial direction. In particular, they appear to be superimposed on larger scale motions. As shown in Figs. 5(a) and 5(b), the lateral and front views of the iso-contours of the scalar field highlight that these large scale motions take the form of spanwise rolls (lateral view) and of plume-like structures (front view). The common picture of these large scale motions is the following. The flow first develops spanwise vortex tubes as a result of a two-dimensional shear instability. The strain field associated with this spanwise vortex pattern amplifies flow field perturbations leading to the formation of vortex tubes aligned with it (see the swirling motions reported in Fig. 4). In turn, these predominantly streamwise vortices interact with the primary spanwise vortices that created them inducing an undulation of their axis of rotation.[20] The lift-up of spanwise vortices within pairs of counter rotating streamwise vortices leads to the formation of spanwise arranged array of mushroom-like structures, see panel 5(b), and, consequently to high- and low-speed streamwise velocity streaks.[21,25] Interestingly, the scalar field highlights that the mixing processes are not able to fill the entire space even within the turbulent core. As shown by the top views in Figs. 5(c) and 5(d), regions of zero concentration of the scalar are observed also within the turbulent core. Obviously, these regions of unmixed flow are more prevalent in the outer regions of the jet.

IV. THREE-DIMENSIONAL SPATIAL CORRELATION FUNCTIONS

The statistical signature of the previously described flow pattern can be studied by means of two-point statistics, such as the velocity correlation function in physical space. This observable allows us to identify the statistically dominant three-dimensional structures of the flow and to quantitatively assess their topology. For the symmetries of the flow, the spatial correlation function for a generic quantity β can be defined as

$$R_{\beta\beta}(r_x, r_y, r_z, z, t) = \frac{\langle \beta'(x, y, z, t)\beta'(x + r_x, y + r_y, z + r_z, t)\rangle}{\langle \beta'\beta'\rangle(z, t)}. \quad (4)$$

Note that in inhomogeneous turbulence, the two-point correlation function lacks an unique definition. The related technical details are reported in the Appendix. Equation (4) highlights that the correlation function, for a fixed time, is defined in a four-dimensional space of separations (r_x, r_y, r_z) and positions (z). For each position (z) within the flow, the spatial correlation function allows us to define the lengths (r_x, r_y, r_z) of the statistically dominant coherent motions. Due to statistical inhomogeneity in the cross-flow direction and to the presence of a mean flow in the streamwise direction, the three-dimensional spatial correlation function (4) among the space of separations is symmetric only in the r_y-direction, i.e.,

$$R_{\beta\beta}(r_x, r_y, r_z, z, t) = R_{\beta\beta}(r_x, -r_y, r_z, z, t). \quad (5)$$

The following analysis of the behavior of the three-dimensional spatial correlation function allows us to describe the shape of statistically relevant flow structures. In order to give a more quantitative description of their size, we will use the quantity ℓ_j defined as the maximum distance between points of a given three-dimensional correlation iso-surface along the j direction and d_j to denote the distance between peaks of positive and negative correlation along the j direction. Accordingly, ℓ_j describes the size of fluctuating velocity structures while d_j both the distance between alternating fluctuating velocity structures or the diameter of vortical structures.[35]

V. STATISTICALLY RELEVANT FLOW STRUCTURES

For reasons of compactness, the analysis of the three-dimensional spatial correlation function of the velocity field is reported in this section for four fixed reference z-locations. As shown in Fig. 1(a) with vertical lines, the selected locations have been chosen in order to characterize the structures of the flow in the inner, production, outer, and external regions of the jet, see Cimarelli *et al.*[31] for a

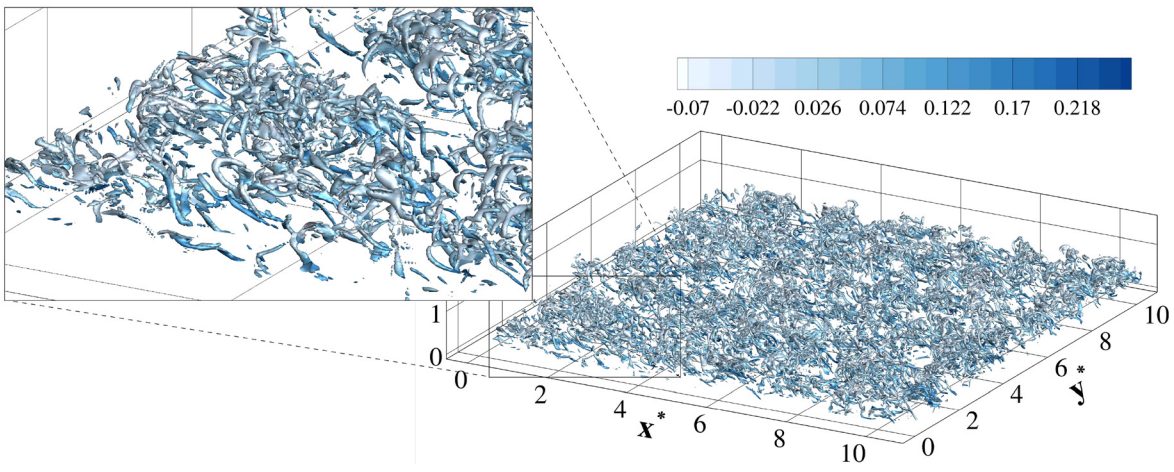

FIG. 4. Iso-surface of swirl, $\boldsymbol{\omega} \cdot \boldsymbol{u}/|\boldsymbol{u}| = \pm 3.6$ colored with streamwise velocity u for $t = 120$.

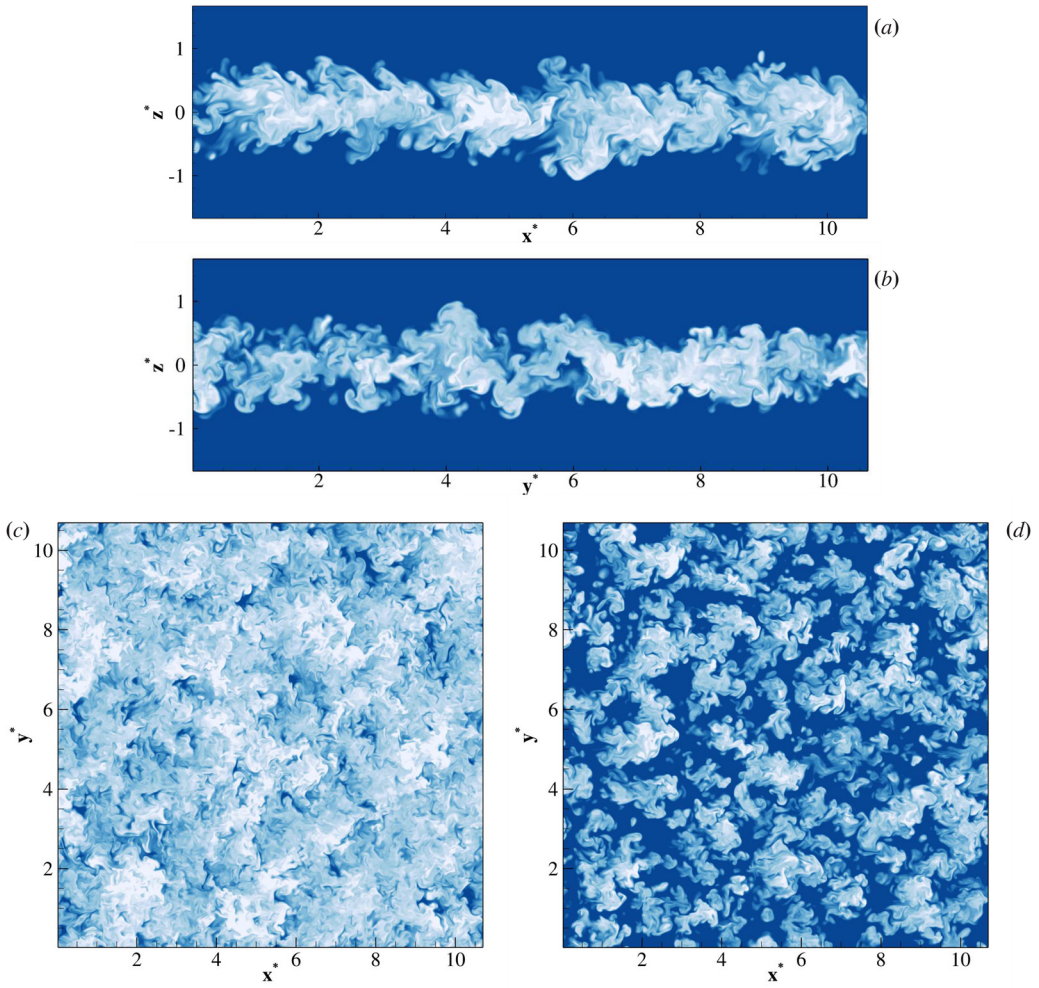

FIG. 5. Iso-contours of the scalar field at $t = 120$ evaluated for a fixed y-plane (a), x-plane (b) and for two fixed z-planes in the core of the jet (c) for $z = 0$ and in the outer region of the jet (d) for $z^* = 0.5$.

description. In the following, these regions will be addressed separately.

It is finally useful to recall that, as shown in Cimarelli *et al.*[31] and discussed in Secs. II A and II B, the flow observables exhibit a clear self-similar behavior for $t > 60$. For this reason, the following analysis of the statistically relevant flow structures is reported in self-similar units denoted with a superscript $*$, see their definition in Sec. II A, and for $t = 120$, so well within the self-similar regime. Accordingly, the reported self-similar size and shape of the three-dimensional correlation functions are expected to be time invariant.

A. Inner region

We start by considering the most relevant turbulent structures populating the jet inner core by studying the behavior of the spatial correlation function at $z^* = 0$. As shown in Fig. 6, the most relevant feature of this region is given by the fact that the intensity of the negative peaks of the correlation function R_{uu} and R_{vv} is very weak, of the order of 5%–7% the maximum value of correlation. Furthermore, these negative peaks are at very large separations far exceeding the jet half-width. Hence, we argue that no vortical structures nor streaky pattern are statistically relevant in this region of the flow. On the contrary, the spatial correlation function R_{ww} shows a significant negative peak of correlation in the streamwise direction of the order of the 17% of the maximum correlation. This behavior is the statistical signature of the large-scale spanwise vortices and will be further analyzed in Secs. V B and V C.

Overall, the scenario described by the spatial correlation function for the jet inner core is similar to isotropic turbulence. No turbulent structures are detected, thus suggesting that turbulent vortices and structures are randomly oriented in this region of the flow such as in isotropic turbulence. The only exception is given by a large-scale signature given by the spanwise vortex structures related to the shear instability. Hence, we argue that randomly oriented turbulent eddies are superimposed on this anisotropic large-scale motion without being significantly modulated.

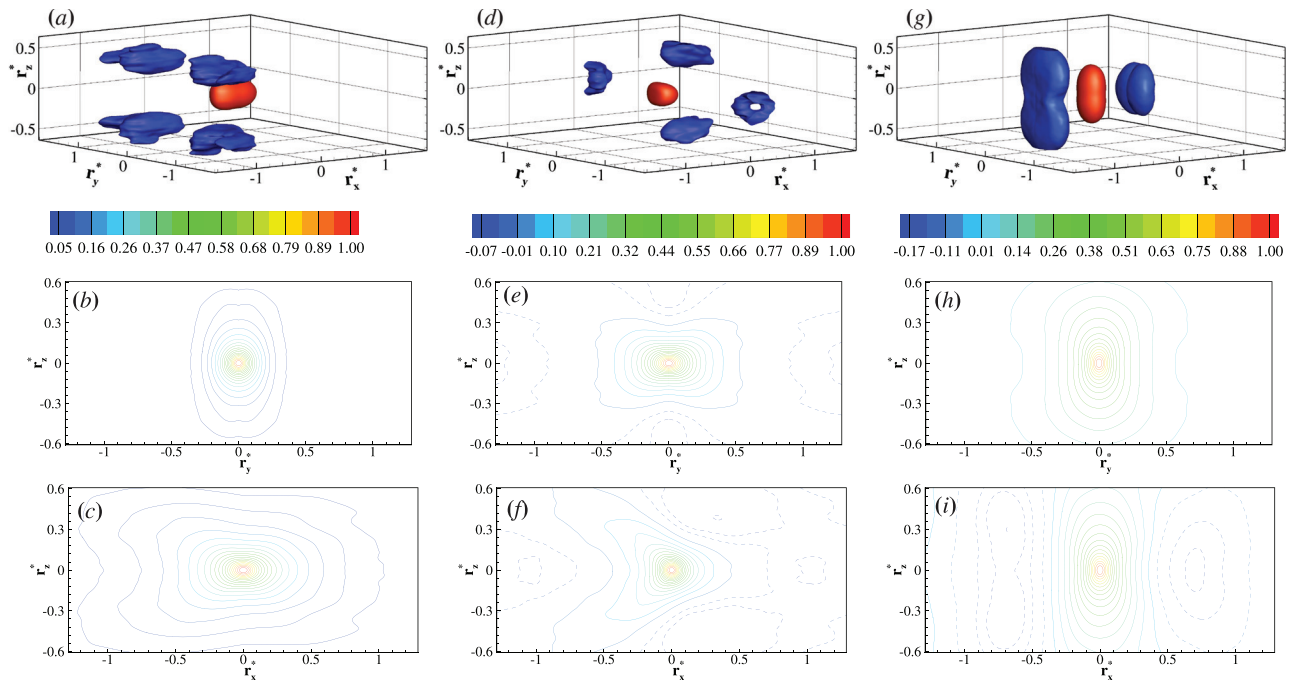

FIG. 6. Three-dimensional spatial correlation function evaluated in the inner region, $z^* = 0$. Left panels (a)–(c): R_{uu}. Central panels (d)–(f): R_{vv}. Right panels (g)–(i): R_{ww}. The top panels (a), (d), and (g) show a three-dimensional view of the (r_x^*, r_y^*, r_z^*)-space by means of two iso-surfaces of positive and negative correlation, i.e., for $R_{\beta\beta} = 0.3R_{\beta\beta}^{\max}$ (red) and for $R_{\beta\beta} = 0.7R_{\beta\beta}^{\min}$ (blue), respectively. Two-dimensional section of the iso-levels of velocity correlations for $r_x^* = 0$, central panels (b), (e), and (h), and for $r_y^* = 0$, bottom panels (c), (f), and (i). Solid lines represent positive values, while dashed lines denote negative values.

B. Production region

We now consider the structure of turbulence in the production region by considering the behavior of the spatial correlation function at $z^* = 0.35$. As reported in Fig. 7, the spatial correlation function R_{uu} shows the presence of high and low streamwise velocity fluctuations alternated in the spanwise direction with a spacing $d_y^* \approx 0.64$. The shape of these structures is elongated in the streamwise direction, $(\ell_x^*, \ell_y^*, \ell_z^*) \approx (1.5, 0.7, 0.9)$. As anticipated in Sec. III, streamwise velocity streaks are associated with the presence of quasi-streamwise vortices, which lift up high velocity fluid. The presence of these structures is unveiled by the behavior of the spatial correlation function R_{vv}. Indeed, as shown in Fig. 7, R_{vv} highlights the presence of vortical motions inclined with respect to the symmetry plane of the jet with an angle $\varphi \approx -31^\circ$. These vortical structures have an elongated shape whose principal axis are (r_τ, r_y, r_η). The size of these structures is $(\ell_\tau^*, \ell_y^*, \ell_\eta^*) \approx (1.34, 0.92, 0.32)$, and the diameter of the corresponding vortical motion is $d_\eta^* \approx 0.4$. Contrary to R_{uu} and R_{vv}, a completely different flow pattern induced by the large-scale spanwise vortex structures is unveiled by the spatial correlation function R_{ww}. As shown in Fig. 7, the shape of these cross-flow structures is elongated in the cross-flow direction, $(\ell_x^*, \ell_y^*, \ell_z^*) \approx (0.7, 1.16, 1.52)$, while the diameter of the corresponding vortical motion is $d_x^* \approx 0.64$. Hence, this vortical motion involves the entire jet region. The strength of this motion cancels out the appearance of negative peaks of correlation in the spanwise direction that we are expecting to see as related to the previously observed inclined vortical motions. This is probably due to the fact that the latter occurs at smaller scales and, hence, is probably less intense with respect to the former.

Overall, we observe that in the production region quasi-streamwise vortical structures inclined -31° with respect to the symmetry plane of the jet exist and are associated with the appearance of a streamwise velocity streak pattern. Considering that this region is also characterized by high levels of mean shear, this structure of turbulence is classically associated with turbulence production mechanisms. The interactions between these structures are superimposed on a larger-scale spanwise vortex motion. The clear matching of the spatial correlation functions reported in Fig. 7 with those reported in Balamurugan *et al.*[36] for the case of a spatially evolving mixing layer actually suggests a possible universality of the type of structures involved in the production of turbulence in free shear flows.

C. Outer region

The structure of turbulence in the outer region at $z^* = 0.82$ is similar to that observed in the production region, i.e., streamwise velocity streaks and inclined vortical motions superimposed on a very-large spanwise vortex motion. The main differences are the size of the structures and their regions of influence. As reported in Fig. 8, the spatial correlation function R_{uu} shows that the streaky pattern is not localized at the same distance from the jet centerline. Streamwise fluctuations in this region are correlated with streamwise fluctuations with opposite sign at inner locations. As it will be shown in Sec. V D,

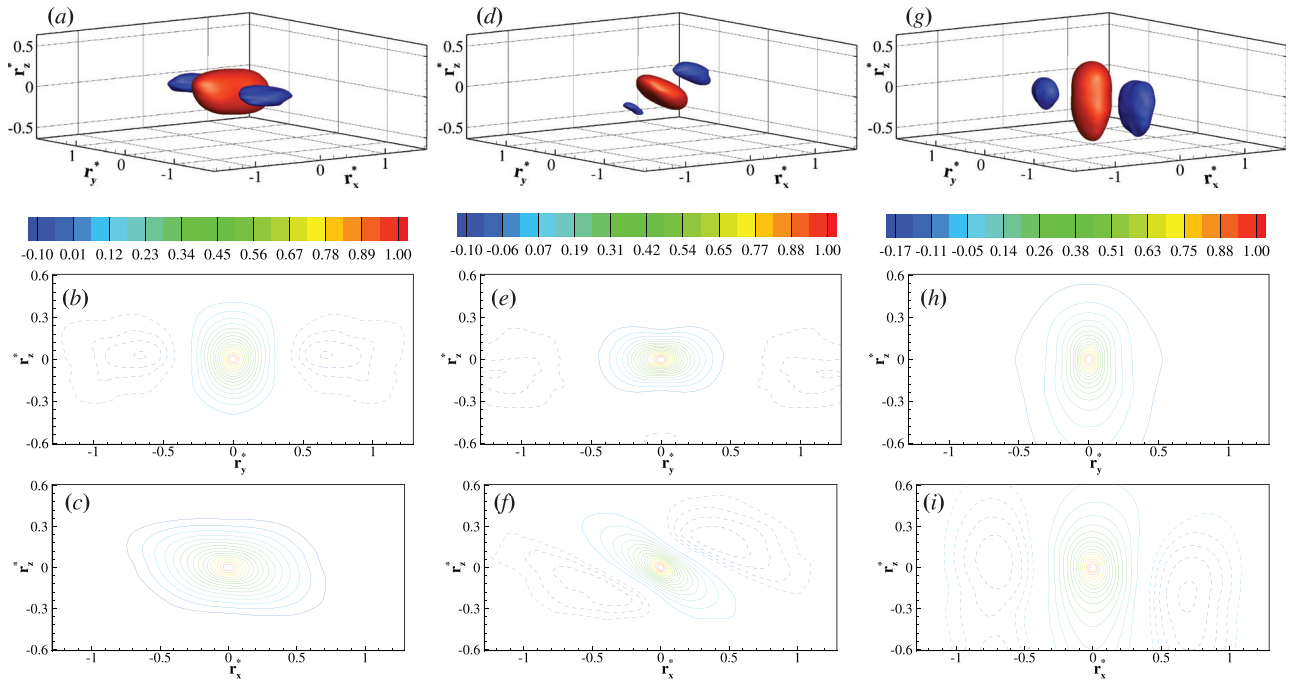

FIG. 7. Three-dimensional spatial correlation function evaluated in the production region, $z^* = 0.35$. Left panels (a)–(c): R_{uu}. Central panels (d)–(f): R_{vv}. Right panels (g)–(i): R_{ww}. The top panels (a), (d), and (g) show a three-dimensional view of the (r_x^*, r_y^*, r_z^*)-space by means of two iso-surfaces of positive and negative correlation, i.e., for $R_{\beta\beta} = 0.2R_{\beta\beta}^{\max}$ (red) and for $R_{\beta\beta} = 0.8R_{\beta\beta}^{\min}$ (blue), respectively. Two-dimensional section of the iso-levels of velocity correlations for $r_x^* = 0$, central panels (b), (e), and (h), and for $r_y^* = 0$, bottom panels (c), (f), and (i). Solid lines represent positive values, while dashed lines denote negative values.

this behavior is associated with the cross-flow mushroom-like shape taken by the very-large spanwise vortex structures that, in turn, is due to the lift-up phenomenon induced by pairs of counter-rotating quasi-streamwise vortices. On the other hand, the spatial correlation function R_{vv} shows that the inclined quasi-streamwise vortices in the outer region have a larger inclination, $\varphi \approx -45^\circ$, and a larger size, $d_\eta^* \approx 0.58$. The spatial correlation function R_{ww} is again dominated by the signature of the spanwise vortex motions. The main difference with respect to the production and inner region is given by the fact that the width of the statistically relevant cross-flow fluctuations is larger and that are correlated with cross-flow fluctuations of opposite sign at inner locations.

The overall scenario of the outer region is similar to that reported in the production region, i.e., inclined vortical structures and streamwise velocity streaks superimposed on a larger-scale spanwise vortical motion. The main difference is given solely to the larger size and inclination of these turbulent structures. We argue that the larger inclination is given by the fact that in this region the direction of strain induced by pairs of spanwise vortices is more inclined than in the production region. The intensity of the production mechanisms in the outer region are smaller than in the production region despite the structures of turbulence are almost the same. This is probably due to the lower mean shear levels reached in the outer region.

D. External region

We consider here the structure of turbulence in the external region of the jet at $z^* = 1.17$. As shown in Fig. 9, the spatial correlation function R_{uu} does not show any more a streaky pattern for the streamwise velocity fluctuations. Streamwise fluctuations are very wide structures $\ell_y^* \approx 3.5$ and are correlated with streamwise fluctuations of opposite sign at inner locations, thus highlighting that in the external region of the flow, the streamwise velocity field is actually dominated by the spanwise vortex motion resulting from the shear instability of the flow. The inclination of these streamwise velocity structures with respect to the symmetry plane of the jet is $\varphi \approx 38^\circ$. Interestingly, R_{uu} exhibits a mushroom-like shape that appears to be the result of a lift-up phenomenon of the very-large spanwise vortex motion of the jet. We argue that the lift-up of very-large spanwise vortices is induced by the action of pairs of counter-rotating quasi streamwise vortices populating the inner regions of the flow as shown in Secs. V B and V C. Accordingly, the mushroom-like shape can be clearly associated with the interaction of the flow motion induced by quasi-streamwise vortices with that of the very-large spanwise vortices.

All the spatial correlation functions show a peak of correlation at inner locations with respect to the detection point, i.e., for negative values of r_z. This shift is particularly large for the spanwise and cross-flow turbulent structures, R_{vv} and R_{ww}, respectively. In particular, we measure that the peak of correlation occurs at $(z + r_z)^* \approx 0.64$ and $(z + r_z)^* \approx 0.52$ for R_{vv} and R_{ww}, respectively. Hence, the spanwise and cross-flow velocity fluctuations in the external region are not a result of local turbulent structures but are given by the motions induced by turbulent structures centered at inner locations. In particular, the spanwise velocity motion in the external region appears as the spanwise velocity spreading induced by the inclined vortical motions populating the outer and production regions. On the other hand, the

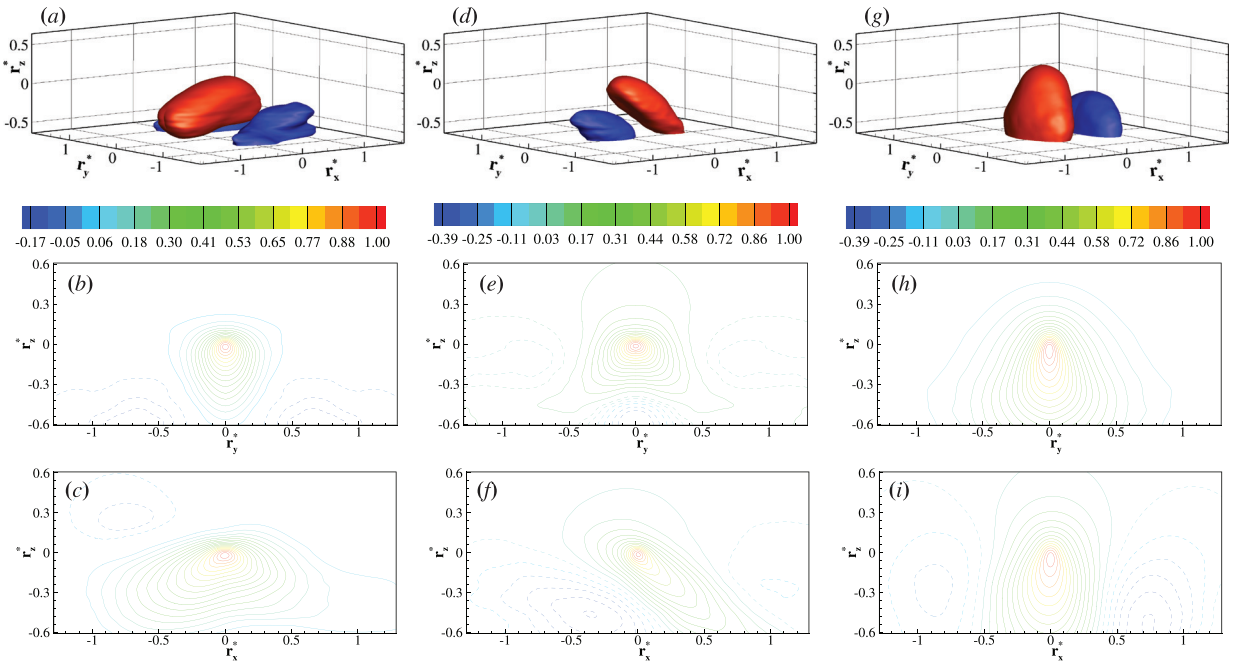

FIG. 8. Three-dimensional spatial correlation function evaluated in the outer region, $z^* = 0.82$. Left panels (a)–(c): R_{uu}. Central panels (d)–(f): R_{vv}. Right panels (g)–(i): R_{ww}. The top panels (a), (d), and (g) show a three-dimensional view of the (r_x^*, r_y^*, r_z^*)-space by means of two iso-surfaces of positive and negative correlation, i.e., for $R_{\beta\beta} = 0.2R_{\beta\beta}^{\max}$ (red) and for $R_{\beta\beta} = 0.5R_{\beta\beta}^{\min}$ (blue), respectively. Two-dimensional section of the iso-levels of velocity correlations for $r_x^* = 0$, central panels (b), (e), and (h), and for $r_y^* = 0$, bottom panels (c), (f), and (i). Solid lines represent positive values while dashed lines denote negative values.

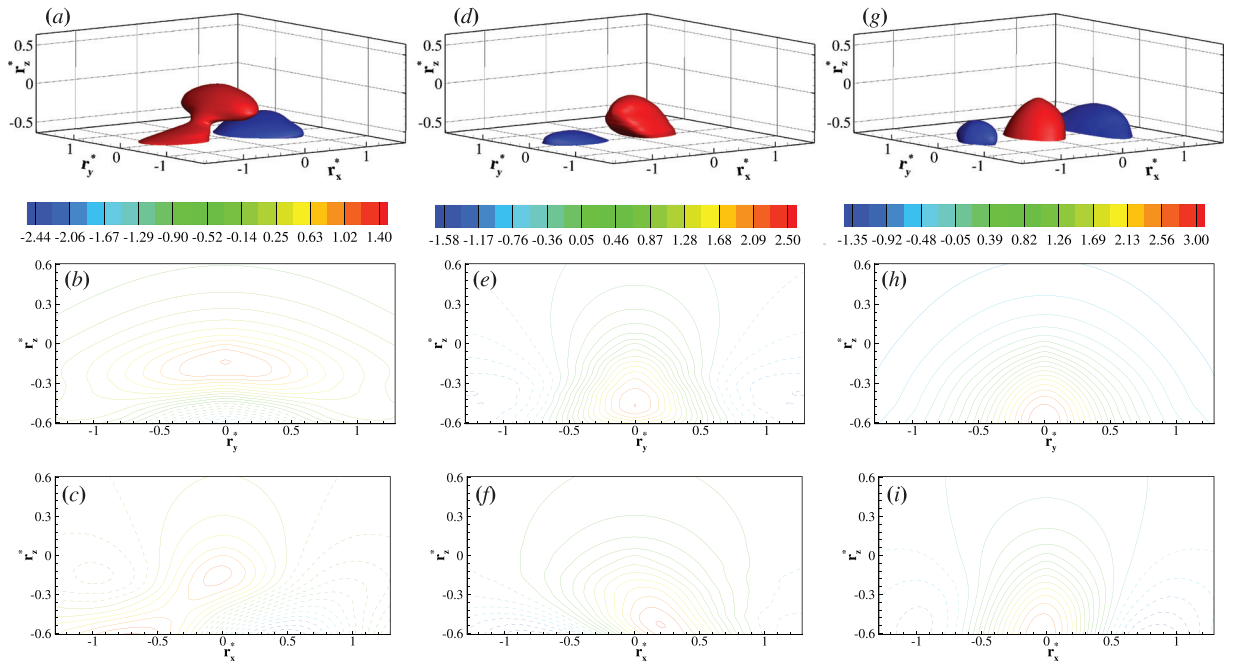

FIG. 9. Three-dimensional spatial correlation function evaluated in the external region, $z^* = 1.17$. Left panels (a)–(c): R_{uu}. Central panels (d)–(f): R_{vv}. Right panels (g)–(i): R_{ww}. The top panels (a), (d), and (g) show a three-dimensional view of the (r_x^*, r_y^*, r_z^*)-space by means of two iso-surfaces of positive and negative correlation, i.e., for $R_{\beta\beta} = 0.5R_{\beta\beta}^{\max}$ (red) and for $R_{\beta\beta} = 0.5R_{\beta\beta}^{\min}$ (blue), respectively. Two-dimensional section of the iso-levels of velocity correlations for $r_x^* = 0$, central panels (b), (e), and (h), and for $r_y^* = 0$, bottom panels (c), (f), and (i). Solid lines represent positive values while dashed lines denote negative values.

cross-flow velocity motion in the external region appears as a result of the flow circulation induced by the spanwise vortex rolls.

Overall, it appears that the motions in the external regions of the jet are induced by the flow circulation generated by turbulent structures populating inner locations. Indeed, the peaks of correlation are reached for significantly negative cross-flow separations $r_z < 0$. In particular, the streamwise and cross-flow fluctuations in the outer region are the result of the interaction of very-large spanwise vortices with quasi-streamwise vortices populating the inner jet regions. Accordingly, the streamwise fluctuations have a mushroom-like shape $\ell_y^* \approx 3.5$ wide and $\varphi \approx 38^\circ$ inclined. This is in agreement with the presence of lift up phenomena of the spanwise vortex rolls that is induced by the flow circulation of pairs of quasi-streamwise vortices whose influence is felt also in the external region of the jet as shown by the spatial correlation function of spanwise velocity.

VI. CONCLUDING REMARKS

Based on direct numerical simulation data of a temporal planar turbulent jet, the structure of turbulence in free-shear flows was analyzed in detail. The instantaneous flow pattern revealed the presence of large-scale motions induced by the flow instability and of small-scale turbulent structures superimposed on it. To characterize the topology of the statistically relevant structures populating the different flow regions, a study of the three-dimensional spatial correlation function was performed. The presence of large spanwise vortices was highlighted. The induced motion is found to be felt in the entire flow field, especially for the cross-flow fluctuations. Superimposed to this large-scale motion, the presence of quasi-streamwise vortices is unveiled in the production and outer regions of the jet. The length of these vortices is $\ell_\tau^* \approx 1.4$ while their inclination and diameter is found to increase by moving from the core to the outer regions of the jet. In particular, we measure, $\varphi \approx -31^\circ$ and $d_\eta^* \approx 0.4$ at $z^* = 0.35$ and $\varphi \approx -45^\circ$ and $d_\eta^* \approx 0.58$ at $z^* = 0.82$. The flow motion induced by pairs of quasi-streamwise vortices is responsible for the lift-up of the large-scale spanwise rolls and for their deformation forming mushroom-like flow structures flanked from below by streamwise velocity streaks. To summarize, the flow topology can be schematized as in Fig. 10. It consists of a spanwise arranged array of intense spanwise vortices whose diameter is $d_x^* \approx 0.64$ and whose width changes with the jet centerline distance from $\ell_y^* \approx 1.1$ to $\ell_y^* \approx 3.5$ due to their cross-sectional mushroom-like shape. These spanwise vortices are flanked from below by counter-rotating pairs of quasi-streamwise vortices that created them. This hairpin-like flow circulation is in turn responsible for the generation of high and low streamwise velocity streaks whose length and width are $\ell_x^* \approx 1.5$ and $\ell_y^* \approx 0.7$.

In conclusion, the present statistical analysis is shown to provide a rigorous description of the coherent structures populating free-shear flows. The emerging qualitative picture is in agreement with several previous observations, such as those of Perry and Tan,[3] Liepmann and Gharib,[4] Bernal and Roshko,[21] Brancher *et al.*,[37] Kantharaju *et al.*[38] On the other hand, the quantitative description given by the correlation functions can be eventually used to assess and calibrate large-scale eddy models, such as that of Philip and Marusic[7] to give a structural prediction of the otherwise disorganized motion in turbulent free-shear flows. As a side result, it is also found that the very large separation of scales occurring in free-shear flows calls for the adoption of very large computational domains in order to capture the interactions between large-scale instability and small-scale turbulence. By increasing the area spanned by the two homogeneous directions, larger domains are also found to improve the statistical convergence of the data.

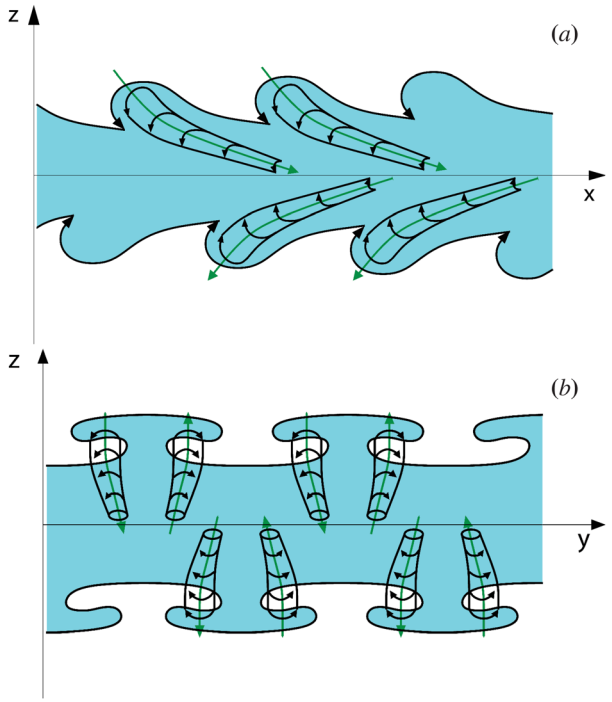

FIG. 10. Schematic of the structure of quasi-streamwise and very-large spanwise vortices. The lateral view (a) highlights the inclination of quasi streamwise vortices inducing the lift-up of the spanwise vortex motion. The green arrow indicates the sense of rotation of the vortices using the right-hand rule. The frontal view (b) highlights how the lift-up of spanwise vortices induced by counter-rotating quasi-streamwise vortices leads to a mushroom-like shape of the spanwise vortex structure itself. To note that this cross-flow pattern leads to a high streamwise velocity streak in between the two counter-rotating vortices and two low streamwise velocity streaks at their sides.

ACKNOWLEDGMENTS

The authors acknowledge the financial support of the Engineering and Physical Sciences Research Council (EPSRC) through the project "Multi-scale dynamics at the turbulent/non-turbulent interface of jets and plumes"—Grant No. EP/R042640/1. Computing time has been provided by the UK National Supercomputing Service ARCHER and by the Supercomputing Wales facility. A.C. wishes to acknowledge the support of the Department of Engineering "Enzo Ferrari" of the University of Modena and Reggio Emilia through the action "FAR dipartimentale 2020/2021."

AUTHOR DECLARATIONS

Conflict of Interest

The authors have no conflicts to disclose.

DATA AVAILABILITY

The data that support the findings of this study are available from the corresponding author upon reasonable request.

APPENDIX: CORRELATION FUNCTIONS IN INHOMOGENEOUS FLOWS

There are two ways to define the spatial correlation function in inhomogeneous flows,

$$R^a_{\beta\beta}(r_x, r_y, r_z, z) = \frac{\langle \beta'(x,y,z)\beta'(x+r_x, y+r_y, z+r_z)\rangle}{\sqrt{\langle \beta'\beta'\rangle(z)\langle \beta'\beta'\rangle(z+r_z)}} \quad \text{(A1)}$$

and

$$R^b_{\beta\beta}(r_x, r_y, r_z, z) = \frac{\langle \beta'(x,y,z)\beta'(x+r_x, y+r_y, z+r_z)\rangle}{\langle \beta'\beta'\rangle(z)}, \quad \text{(A2)}$$

where, without loss of generality, we have considered inhomogeneity in a single direction z as it is for the temporal jet and statistical stationarity. By using the rearrangement inequality, it is possible to demonstrate that

$$\langle \beta'(x,y,z)\beta'(x+r_x, y+r_y, z+r_z)\rangle \le \sqrt{\langle \beta'\beta'\rangle(z)\langle \beta'\beta'\rangle(z+r_z)}, \quad \text{(A3)}$$

so that we have

$$R^a_{\beta\beta} \le 1,$$

while

$$R^b_{\beta\beta} \le \sqrt{\frac{\langle \beta'\beta'\rangle(z+r_z)}{\langle \beta'\beta'\rangle(z)}}.$$

The two definitions (A1) and (A2) are equal in statistically homogeneous flows since $\langle \beta'\beta'\rangle(z) = \langle \beta'\beta'\rangle(z+r_z)$ and, hence, satisfy the same constraint, i.e., $R^a_{\beta\beta} \le 1$ and $R^b_{\beta\beta} \le 1$. However, in inhomogeneous flows, the two definitions differ from each other and, in particular, the constraint for $R^b_{\beta\beta}$ is in general different from 1. Thus, the advantage of the first definition is that the constraint $R^a_{\beta\beta} \le 1$ is always satisfied, thus making it easier to recognize what is correlated and what is not. On the other hand, the second definition has the advantage that all the observed variations in the space of separations can be attributed uniquely to the correlation function itself, i.e., $\langle \beta'(x,y,z)\beta'(x+r_x, y+r_y, z+r_z)\rangle$, and not to variations of the statistical variance between the two points. This is the reason why we decided to use the second definition in the present work.

REFERENCES

[1] P. Holmes, J. L. Lumley, G. Berkooz, and C. W. Rowley, *Turbulence, Coherent Structures, Dynamical Systems and Symmetry* (Cambridge university Press, 2012).
[2] P. E. Dimotakis, R. C. Miake-Lye, and D. A. Papantoniou, "Structure and dynamics of round turbulent jets," Phys. Fluids **26**, 3185–3192 (1983).
[3] A. E. Perry and D. K. M. Tan, "Simple three-dimensional vortex motions in coflowing jets and wakes," J. Fluid Mech. **141**, 197–231 (1984).
[4] D. Liepmann and M. Gharib, "The role of streamwise vorticity in the near-field entrainment of round jets," J. Fluid Mech. **245**, 643–668 (1992).
[5] S. Cannon, F. Champagne, and A. Glezer, "Observations of large-scale structures in wakes behind axisymmetric bodies," Exp. Fluids **14**, 447–450 (1993).
[6] C. B. da Silva, R. J. N. Dos Reis, and J. C. F. Pereira, "The intense vorticity structures near the turbulent/non-turbulent interface in a jet," J. Fluid Mech. **685**, 165 (2011).
[7] J. Philip and I. Marusic, "Large-scale eddies and their role in entrainment in turbulent jets and wakes," Phys. Fluids **24**, 055108 (2012).
[8] C. B. da Silva, J. C. R. Hunt, I. Eames, and J. Westerweel, "Interfacial layers between regions of different turbulence intensity," Annu. Rev. Fluid Mech. **46**, 567–590 (2014).
[9] K. R. Sreenivasan, R. Ramshankar, and C. Meneveau, "Mixing, entrainment and fractal dimensions of surfaces in turbulent flows," Proc. R. Soc. London, Ser. A **421**, 79–108 (1989).
[10] A. K. M. F. Hussain, "Coherent structures and turbulence," J. Fluid Mech. **173**, 303–356 (1986).
[11] C. B. da Silva and R. J. N. dos Reis, "The role of coherent vortices near the turbulent/non-turbulent interface in a planar jet," Philos. Trans. R. Soc., A **369**, 738–753 (2011).
[12] T. Watanabe, R. Jaulino, R. R. Taveira, C. B. da Silva, K. Nagata, and Y. Sakai, "Role of an isolated eddy near the turbulent/non-turbulent interface layer," Phys. Rev. Fluids **2**, 094607 (2017).
[13] A. Cimarelli and G. Boga, "Numerical experiments on turbulent entrainment and mixing of scalars," J. Fluid Mech. **927**, A34 (2021).
[14] L. K. Su and N. T. Clemens, "The structure of fine-scale scalar mixing in gas-phase planar turbulent jets," J. Fluid Mech. **488**, 1–29 (2003).
[15] C. B. da Silva, "The behavior of subgrid-scale models near the turbulent/non-turbulent interface in jets," Phys. Fluids **21**, 081702 (2009).
[16] C. B. da Silva, D. C. Lopes, and V. Raman, "The effect of subgrid-scale models on the entrainment of a passive scalar in a turbulent planar jet," J. Turbl. **16**, 342–366 (2015).
[17] C. B. da Silva and O. Mètais, "On the influence of coherent structures upon interscale interactions in turbulent plane jets," J. Fluid Mech. **473**, 103–145 (2002).
[18] C. B. da Silva and O. Métais, "Vortex control of bifurcating jets: A numerical study," Phys. Fluids **14**, 3798–3819 (2002).
[19] H. Choi, W.-P. Jeon, and J. Kim, "Control of flow over a bluff body," Annu. Rev. Fluid Mech. **40**, 113–139 (2008).
[20] J. Jiménez, "A spanwise structure in the plane shear layer," J. Fluid Mech. **132**, 319–336 (1983).
[21] L. P. Bernal and A. Roshko, "Streamwise vortex structures in plane mixing layers," J. Fluid Mech. **170**, 499–525 (1986).
[22] P. Nogueira, A. Cavalieri, P. Jordan, and V. Jaunet, "Large-scale streaky structures in turbulent jets," J. Fluid Mech. **873**, 211–237 (2019).
[23] K. Sasaki and M. Kiya, "Three-dimensional vortex structure in a leading-edge separation bubble at moderate Reynolds numbers," J. Fluids Eng. **113**, 405–410 (1991).
[24] M. Kiya and K. Sasaki, "Structure of large-scale vortices and unsteady reverse flow in the reattaching zone of a turbulent separation bubble," J. Fluid Mech. **154**, 463–491 (1985).
[25] J. C. Lasheras and H. Choi, "Three-dimensional instability of a plane free shear layer: An experimental study of the formation and evolution of streamwise vortices," J. Fluid Mech. **189**, 53–86 (1988).
[26] A. Cimarelli, A. Leonforte, and D. Angeli, "On the structure of the self-sustaining cycle in separating and reattaching flows," J. Fluid Mech. **857**, 907–936 (2018).
[27] J. Craske and M. van Reeuwijk, "Energy dispersion in turbulent jets. Part 1. Direct simulation of steady and unsteady jets," J. Fluid Mech. **763**, 500–537 (2015).
[28] R. W. C. P. Verstappen and A. E. P. Veldman, "Symmetry-preserving discretization of turbulent flows," J. Comput. Phys. **187**, 343–368 (2003).
[29] M. van Reeuwijk and M. Holzner, "The turbulence boundary of a temporal jet," J. Fluid Mech. **739**, 254–275 (2014).
[30] C. B. da Silva and J. C. F. Pereira, "Invariants of the velocity-gradient, rate-of-strain, and rate-of-rotation tensors across the turbulent/nonturbulent interface in jets," Phys. Fluids **20**, 055101 (2008).
[31] A. Cimarelli, J.-P. Mollicone, M. van Reeuwijk, and E. De Angelis, "Spatially evolving cascades in temporal planar jets," J. Fluid Mech. **910**, A19 (2021).
[32] R. D. Moser and M. M. Rogers, "Mixing transition and the cascade to small scales in a plane mixing layer," Phys. Fluids A **3**, 1128–1134 (1991).
[33] P. E. Dimotakis, "The mixing transition in turbulent flows," J. Fluid Mech. **409**, 69–98 (2000).
[34] A. Attili and F. Bisetti, "Statistics and scaling of turbulence in a spatially developing mixing layer at $\mathrm{Re}_\lambda = 250$," Phys. Fluids **24**, 035109 (2012).

[35]J. Sillero, J. Jiménez, and R. Moser, "Two-point statistics for turbulent boundary layers and channels at Reynolds numbers up to $\delta^+ \approx 2000$," Phys. Fluids **26**, 105109 (2014).
[36]G. Balamurugan, A. Rodda, J. Philip, and A. C. Mandal, "Characteristics of the turbulent non-turbulent interface in a spatially evolving turbulent mixing layer," J. Fluid Mech. **894**, A4 (2020).
[37]P. Brancher, J. M. Chomaz, and P. Huerre, "Direct numerical simulations of round jets: Vortex induction and side jets," Phys. Fluids **6**, 1768–1774 (1994).
[38]J. Kantharaju, R. Courtier, B. Leclaire, and L. Jacquin, "Interactions of large-scale structures in the near field of round jets at high Reynolds numbers," J. Fluid Mech. **888**, A8 (2020).